ISSN: 2414-1895 DOI: 10.6919/ICJE.202601_12(1).0003

Hexagonal Core Photonic Crystal Fiber Efficiently Sensing Illegal Drugs and Cyanides in THz Regime

She Li*, Han Ding, Yingying Song, Jinpei Wang, Feng Wang, Hongwei Ding, and Lanlan Xu

College of Science, Heilongjiang University of Science and Technology, Harbin, 150022, China

*Corresponding author email: lishe1979@163.com

Abstract

Terahertz (THz) photonic crystal fiber (PCF) sensing has significant potential for portable, integrated and rapid detection, particularly for on-site applications in public areas, because of the low photon energy, strong penetration ability of THz wave and the tailoring structure of PCF. THz-PCF sensing can be used to detect illegal drugs and cyanide, both of which are harmful to the human body. This paper investigates the sensing characteristics of THz-PCF with a hexagonal core using the finite element method (FEM) and analyzes the feasibility of the PCF for detecting illegal drugs and cyanide. The results showed that the relative sensitivities respectively reach to 99.482%, 99.301%, 99.854%, 99.689%, 98.404%, and 97.185% for amphetamine, cocaine, ketamine, morphine, sodium cyanide (NaCN) and potassium cyanide (KCN) at 1.5 THz, and the PCF has an extremely low confinement loss. This indicates its promising potential for the detection of illegal drugs and cyanide.

Keywords

Terahertz; Photonic Crystal Fiber; Illegal Drug; Cyanide; Sensing.

1. Introduction

Terahertz (THz) refers to a unique electromagnetic wave with a frequency range from 0.1 THz to 10 THz [1], positioned between microwave and infrared frequencies [2]. Due to the low photon energy and strong penetration ability [3], THz waves are increasingly used in various fields, such as security inspection [4], concentration detection [5], biomedical sensing [6, 7], THz polarization detection [8, 9], medical diagnosis [10] and so on. Combining other optical devices, THz optical devices have some special applications, especially the THz photonic crystal fiber (PCF) that is a novel type of optical fiber that utilizes the periodic structure of photonic crystals to control and guide the transmission of optical signals, and offer some advantages including low loss, high birefringence and single mode transmission [11-13], making it highly promising for optical communication and sensing applications.

Compared to traditional optical fibers, PCF provides additional benefits in optical communication and sensing field by altering the size and shape of the air holes in the core and cladding regions. In recent years, THz-PCF has been increasingly used in sensing applications due to its unique optical properties and exceptional sensing capabilities [14]. THz-PCF emerges from the integration of THz electromagnetic waves and PCF, and can be applied in biomedical sensing, solution concentration detection, environmental monitoring, and more. The extremely low radiation energy of THz waves enables non-destructive detection of cancer cell [15], DNA [16], protein [17], and other biological materials.

ISSN: 2414-1895 DOI: 10.6919/ICJE.202601_12(1).0003

In 2017, Islam et al developed a PCF sensor operating in the THz band to detect water, ethanol, and benzene, achieving relative sensitivity of 85.6%, 85.7%, and 85.9%, respectively [18]. However, the PCF has complex structure and did not consider the effective material loss. In 2018, they investigated the sensing performance of two PCFs with different cores in the terahertz band using Zeonex as the background material, which not only possessed better birefringence characteristics but also lower bending loss. But the relative sensitivities for HCN obtained with the two sensors were only 85.85% and 77.5%, respectively [19].

In 2020, Tahhan et al [20] designed a pentagonal core and cladding PCF-based sensor, the proposed fiber produces a large effective mode area, negligible confinement loss, and extremely low bending and effective material losses. However, the relative sensitivities at 1 THz were only 79.840%, 80.256% and 81.417% for cocaine, amphetamine and ketamine, respectively. In the same year, Bulbul A. A. M. et al [21] designed a highly sensitive PCF for illegal drugs detection, the values of relative sensitivity are 92.34%, 90.72%, 94.91%, and 97.84% at 1.6 THz for amphetamine, cocaine, ketamine and morphine respectively. Nevertheless, the core power fraction and numerical aperture did not consider. In 2023, Monir M. K. et al proposed a PCF sensor with a hexagonal cladding structure, primarily used for detecting amphetamine, cocaine, and ketamine [22]. The relative sensitivity for these substances were 89.50%, 85.50%, and 90.20% at 1 THz, and the confinement loss lowed to 6.20×10^{-8}dB/m, 7.10×10^{-8}dB/m, and 6.40×10^{-8}dB/m, respectively. But the relative sensitivity is relatively low, and the numerical apertures did not involve.

Urine, blood, saliva, sweat, and hair are the most commonly used biological samples for detecting the presence of illegal drugs or lesions in the human body. However, urine and saliva tests are sometimes inaccurate, while blood testing is considered a more reliable method [23]. Cyanide detection is more complex and is less portable and more restrictive, although it is more accurate [24]. Therefore, this paper investigates sensing characteristics of a novel PCF with a hexagonal core structure. In the following section, we detail the structural design and material selection that underpin this PCF's high sensitivity and low loss characteristics. Results demonstrate that the proposed PCF exhibits extremely high relative sensitivity, negligible confinement loss, and lower effective material loss. These sensing properties make the proposed PCF highly suitable not only for detecting chemical substances but also for sensing other biomolecules.

2. PCF Model

The cross-sectional structure of the Zeonex-based PCF sensor is shown in Figure 1(a), featuring a hexagonal core. The cladding is divided into three air holes by three support strips, forming a fan-shaped structure and decreasing the use of Zeonex so that more light is confined to the analyte-filled core to enhance the interaction between light and analyte to increase the relative sensitivity. Topas [25] and Zeonex [26] are the two dominant materials used in THz-PCF sensing. In this paper, we chose Zeonex as the background material for the PCF. Because it has a smaller refractive index with a constant 1.53 across a wide range of THz frequencies [27], lesser impurity content, higher thermal resistance, and a lower loss tangent compared to Topas. Additionally, Zeonex has lower specific gravity, higher chemical resistance at high temperatures, greater transparency, a lower melt flow index, and other favorable properties [28]. These characteristics make it more suitable for high-quality fiber stretching. Furthermore, Zeonex has a minimum material absorption loss of 0.2 cm^{-1} [29].

The finite element method (FEM) is selected to investigate the sensing characteristics of PCF in chemical substance analysis. In the simulation, a perfectly matched layer (PML) is added around the outer boundary of the PCF to prevent light reflection and protect the PCF from the external environment [30], as shown in Fig. 1(a) The PCF has a radius of 1350μm and a PML with a thickness of 10% of the PCF's radius as the absorbing boundary, the hexagonal core has an inner diameter D_1 and an outer diameter D_2 of 760μm, the thickness of the support strip in the cladding air holes is D_3=40μm, the distance between the cladding air holes and the PML is D_4=70μm, and the thickness of the core wall is denoted as h.

ISSN: 2414-1895 DOI: 10.6919/ICJE.202601_12(1).0003

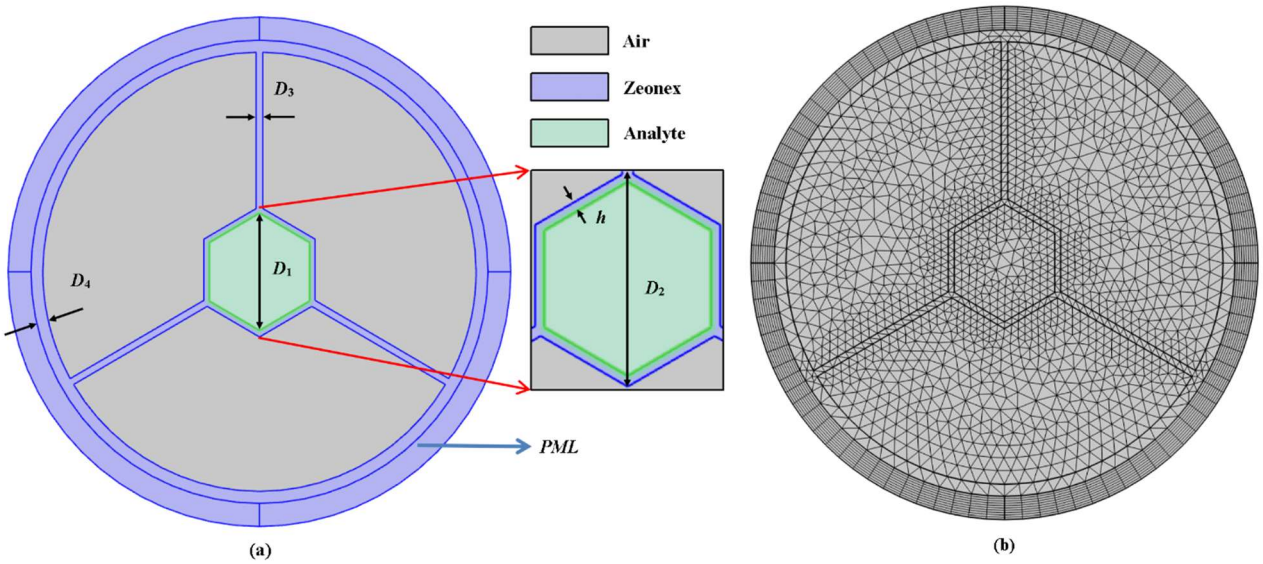

Fig. 1 Schematic of the cross-section of the PCF (a) and Schematic of mesh division (b)

The delineation of the mesh is crucial for solving the relevant properties of the PCF, as shown in Fig. 1(b), where the mesh is divided into two parts for the complete mesh with 2982 domain elements and 512 boundary elements. This mesh pattern ensures a higher number of domains and boundary elements in the core and cladding, which is conducive to effective sensing characteristic analysis of the fiber. The following chemicals and illegal drugs were chosen as analytes: amphetamine (n=1.518), cocaine (n=1.5022), ketamine (n=1.562), morphine (n=1.54), NaCN (n=1.45), and KCN (n=1.41). Here, it is assumed that the refractive indices of the chemicals remains constant over the operating frequency range, and the absorption of THz electromagnetic waves by the chemicals is not considered.

Fig. 2 shows the mode field distribution for the six chemicals at optimum frequency with 1.5 THz for the four illegal drugs and two cyanides. From the figure, it can be seen that the mode field are well confined into the core, which enables strong interaction between the electromagnetic waves and the analytes. Additionally, it is highest at the center of the core and decreases gradually along radial direction. As a result, the relative sensitivity of the proposed sensing PCF will be higher.

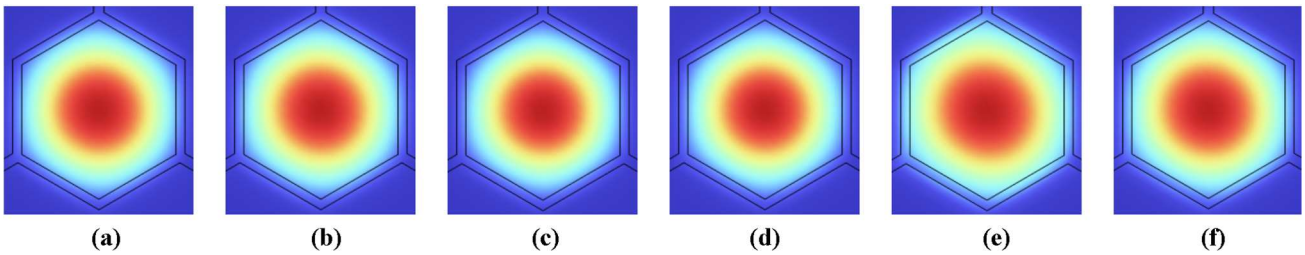

Fig. 2 Mode field distribution in the proposed PCF for (a) amphetamine, (b) cocaine, (c) ketamine, (d) morphine, (e) NaCN, and (f) KCN at 1.5 THz

The substance to be measured can be injected into the core of any PCF by using a selective filling method [31]. The THz-PCF studied can be practically fabricated using common methods, such as capillary stacking [32], stack and draw [33], drilling [34], and sol-gel technology [35]. Further, the combination of extrusion technology [36] and 3D printing [37] provides a technological basis for fabricating THz-PCF with more complex structure, which have highly cost-effective and almost negligible differences between the actual manufactured fiber and the perfect fiber structure. Therefore, the perfect PCF can be only considered in this paper when the last scheme is used.

ISSN: 2414-1895 DOI: 10.6919/ICJE.202601_12(1).0003

3. Numerical and Mathematical Methods

The effective refractive index (ERI) of guided mode is defined as the ratio of the wavelength of the THz wave in vacuum to its wavelength inside the fiber core [38]. For refractive index-guided fibers, the refractive index of the core must be higher than that of the cladding so that the light wave can propagate via total internal reflection, thereby limiting the maximum amount of electromagnetic power within the core. The ERI is given by the following equation [38]:

$$n_{eff} = \lambda_0 / \lambda \tag{1}$$

where λ and λ_0 respectively denote the wavelength of the THz wave in the analyte and vacuum.

Relative sensitivity (RS) is a key performance metric for evaluating PCF biosensing characteristics, which is proportional to the amount of power present in the fiber core and can be expressed by equation (2)[39]:

$$S = \left(n_r / n_{eff} \right) \times P \tag{2}$$

where S is the relative sensitivity, n_r denotes the refractive index of the analytes to be measured in the core, and P is the percentage of light interacting with the sample and can be calculated by the following formula [39]:

$$P = \frac{\int_{Analyte} \mathrm{Re}\left(H_y E_x - H_x E_y \right) dxdy}{\int_{Total} \mathrm{Re}\left(H_y E_x - H_x E_y \right) dxdy} \times 100\% \tag{3}$$

where E_x and E_y are the orthogonal electric field in the cross-section of the fiber, while H_x and H_x stand for the corresponding magnetic field components.

Effective material loss (EML), also known as absorption loss, refers to absorb part of the electromagnetic wave energy by the background material, and is expressed by [40]:

$$\alpha_{eff} = \sqrt{\frac{\varepsilon_0}{\mu_0}} \left(\frac{\int_{A_{mat}} n_{mat} |E|^2 \alpha_{mat} dA}{2 \int_{all} S_z dA} \right) \tag{4}$$

Here n_{mat} and α_{mat} are the refractive index and absorption loss of Zeonex, μ_0 and ε_0 indicate the permeability and permittivity in vacuum, S_Z is the z component of the Poynting vector, and $Amat$ represents the analytes area in the cross-section of the fiber.

Confinement Loss (CL) is also a pivotal factor, which describe the power leakage from the core to the cladding region, and can be calculated as [41]:

$$\alpha_{CL} = \left(4\pi f / c \right) * \mathrm{Im}(n_{eff}) \quad \mathrm{cm}^{-1} \tag{5}$$

where f is the operating frequency and $\mathrm{Im}(n_{eff})$ is the imaginary part of the ERI.

ISSN: 2414-1895 DOI: 10.6919/ICJE.202601_12(1).0003

Core power fraction (CPF) primarily measures the power of electromagnetic waves passing through the core region. A higher core power fraction indicates better performance of the PCF. It can be calculated as [42]:

$$\eta = \frac{\int_{core} SzdA}{\int_{all} SzdA} \tag{6}$$

Effective mode area (EMA) represents the size of the mode field and the degree of power concentration, and can be expressed as[43]:

$$A_{eff} = \frac{\left[\int I(x,y)dxdy\right]^2}{\int I^2(x,y)dxdy} = \frac{\left[\iint |E(x,y)|^2 dxdy\right]^2}{\iint |E(x,y)|^4 dxdy} \tag{7}$$

where $I(x,y) = |E(x,y)|^2$ indicates the intensity of the electric field.

Numerical aperture (NA) is a parameter that indicates the ability of the fiber's end face to receive light. To ensure that light waves are strictly confined to the core area, the refractive index of the fiber core must be higher than that of the cladding. NA can be expressed using the following equation [44]:

$$NA = \frac{1}{\sqrt{1 + \frac{\pi A_{eff} f^2}{c^2}}} \tag{8}$$

where A_{eff} is the EA.

4. Results and Discussion

The effect of the analyte's refractive index on the properties of the fiber was first investigated. The analyte's refractive indices were simulated from 1.3 to 1.6 at 1.5 THz, with a step size of 0.05, as shown in Fig. 3, where the ERI, EA, RS, CPF, EML, and CL were analyzed and demonstrated the PCF suiting for substance analysis.

Fig. 3(a), (b), and (c) show that the ERI, RS and CPF increase as the refractive index of the analyte increases. And they respectively trend to the same values at the higher refractive index, where the refractive index of analtye's is near to, even larger than that of Zeonex that the higher refractive index of analyte's confines the more THz waves to the core region due to the characteristics of the index-guided fiber. It is also observed the RS and CPF are larger with increase of the core inner diameter because of more analyte to interact with the THz waves, while the ERI is the opposite at lower refractive indices since the refractive index of analyte is smaller than that of Zeonex. Fig. 3(d), (e), and (f) illustrate that the EA, EML and CL decrease as the refractive index increases, be higher refractive index enables more effective confinement of THz waves within the core region and can prevents it diffuse into the cladding. At lower refractive indices, an increase in core inner diameter results in a decrease in EA, and the opposite occurs at higher refractive indices due to the change in the relation between the refractive index of the analyte and the background material. The EML decreases with increase of core inner diameter because of a decrease in the filling rate of background material. While there is no apparent significant change in CL, because it mainly depends on the structure of the cladding. Thus, it is concluded that the larger the core area, the larger the CPF, the smaller EML and the higher the sensitivity, and the CLs lie in lower position.

ISSN: 2414-1895 DOI: 10.6919/ICJE.202601_12(1).0003

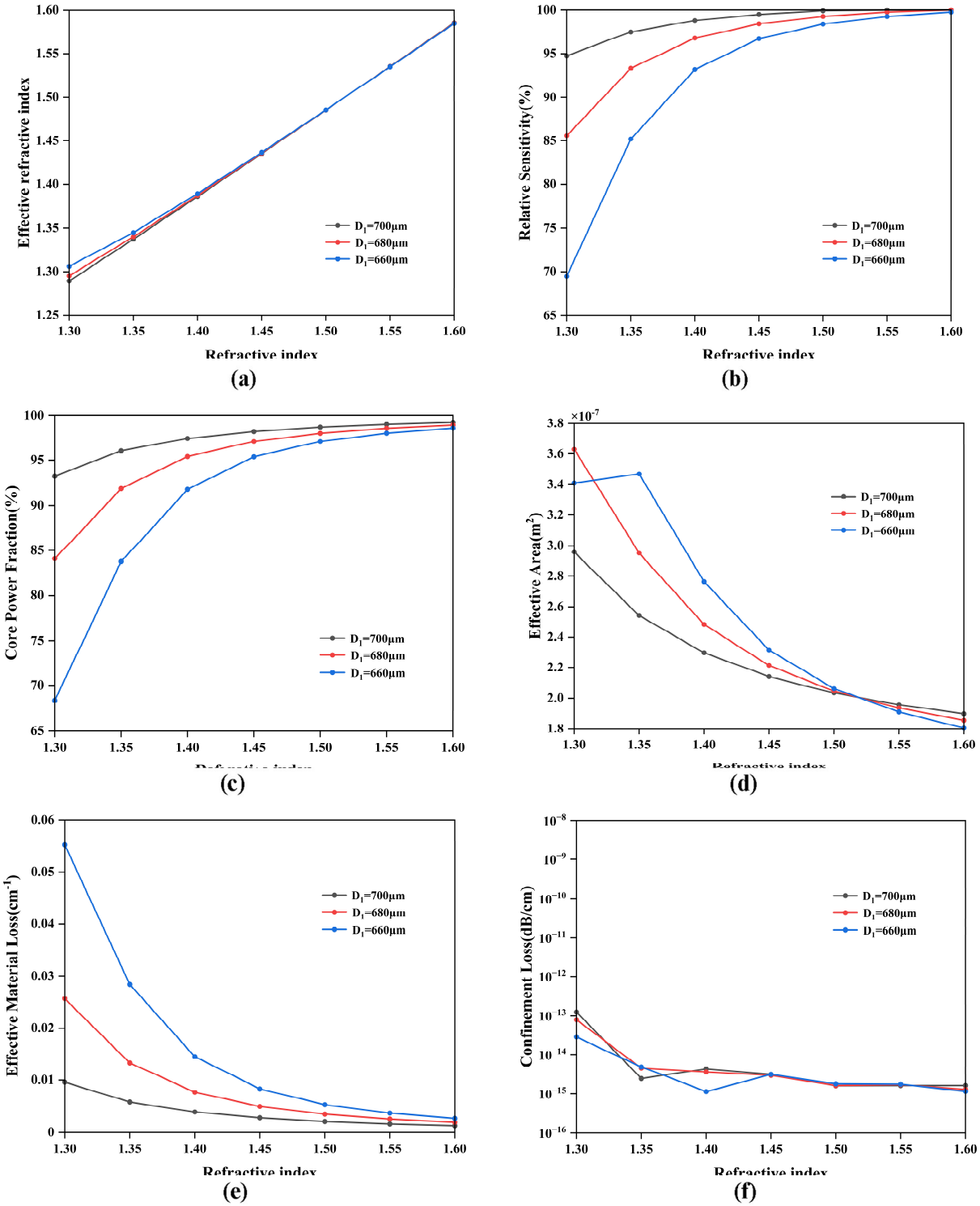

Fig. 3 The variation of (a) ERI, (b) EML, (c) CL, (d) CPF, (e) CPF, (f) CL with analyte's refractive index at 1.5 THz

Fig. 4 presents the mode field contour plots of analytes with different refractive indices at 1.5 THz. It is evident that a higher refractive index results in denser mode field contours to the center of the core indicating a stronger ability to confine THz waves which is agree with Fig. 3(c).

Further, Fig. 3 can demonstrate higher RS, CPF and lower EML and CL with refractive indices in the range of 1.4 to 1.6, while in Fig. 4(a), it can be seen that the mode field contours are denser at the edge of the core for n=1.3. Therefore, the PCF studied in this work can be used to analyze amphetamine, cocaine, ketamine, morphine, NaCN, and KCN.

Volume 12 Issue 1, 2026
DOI: 10.6919/ICJE.202601_12(1).0003

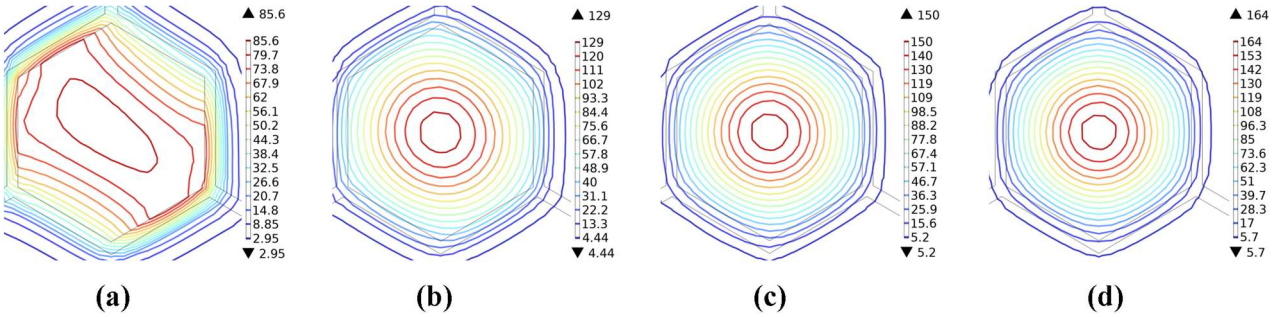

Fig. 4 The contour plots of the mode field for analytes with different refractive indices at 1.5 THz: (a) n=1.3, (b) n=1.4, (c) n=1.5, (d) n=1.6

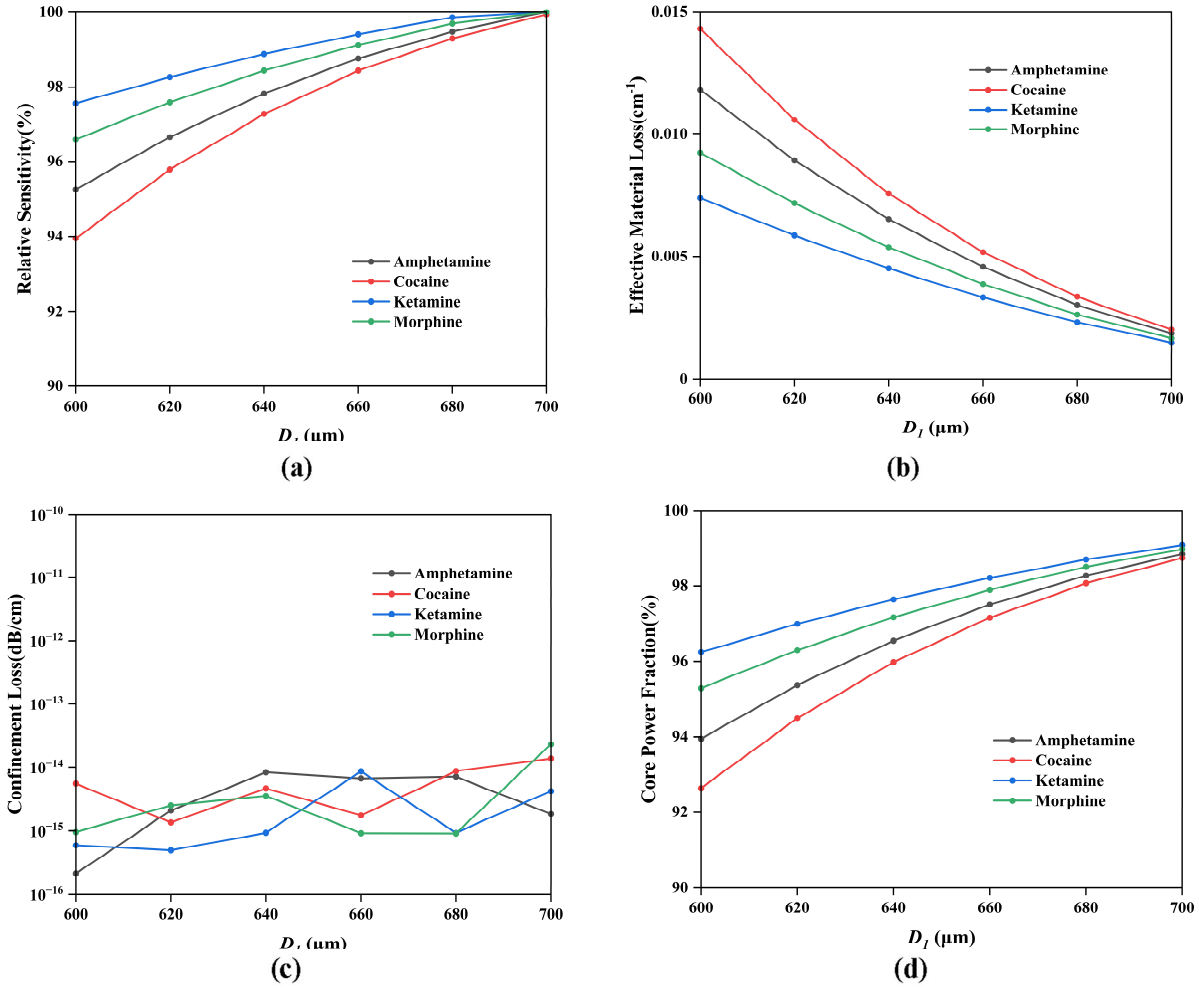

Fig. 5 The variation of the properties of four illegal drugs with core inner diameter at 1.5 THz: (a) RS, (b) EML, (c) CL, (d) CPF

The four important properties of the chemical substances are then analyzed with respect to the core inner diameter. Four illegal drugs are used as examples to determine the optimum core inner diameter for this PCF, based on their RS, EML, CL, and CPF, with a step size of 20μm. The variation of RS and EML with the core inner diameter for the four illegal drugs at a frequency of 1.5 THz is shown in Fig. 5(a) and (b). It can be observed that the RSs increases as the core inner diameter increases. This is because a larger core space allows more volume of the liquid analyte to be filled, which generally enhances the interaction between the analyte and the electromagnetic waves in the core, thereby increasing RS. Under optimal parameters, the RS values for amphetamine, cocaine, ketamine,

ISSN: 2414-1895 DOI: 10.6919/ICJE.202601_12(1).0003

and morphine are all above 99% when $D_1 \geq 680\mu m$. Fig. 5(b) shows that a reduction in EML as the core inner diameter increases since the more electromagnetic waves confined to the analyte of the core. Under larger D_1, the EMLs for amphetamine, cocaine, ketamine, and morphine remain at a very low level

There is no significant difference in the CLs of the four illegal drugs at different core inner diameters. As the core inner diameter increases from 600μm to 700μm, the CL fluctuates within a stable range, as shown in Fig. 5(c). This indicates that the change in the core inner diameter has minimal impact on CL. Under the optimal parameters, the CL for amphetamine, cocaine, ketamine, and morphine can be considered negligible. Fig. 5(d) shows that the CPF of the four illegal drugs increases with the core inner diameter. This is because a larger core can accommodate more analytes and confine the electromagnetic waves to the core, leading to an increase in the core power fraction. Under larger D_1, the CPFs for all four illegal drugs approach or even exceed 98%.

From the analysis of Fig. 3 and Fig. 5, it can be concluded that changes in the core inner diameter have a greater impact on the properties of the PCF model in this study. Although the properties are optimal when the core inner diameter is 700μm, the core wall thickness should not be too thin to ensure the structural stability of the PCF structure. Therefore, in this paper 680μm is chosen as the most suitable core inner diameter for the PCF model.

After determining the optimal core inner diameter, the characteristics of the six analytes within the operating frequency range will be analyzed, as shown in Fig. 6, it can be observed that the ERI of the analytes increases with the operating frequency. This is because the higher frequency electromagnetic waves have shorter wavelengths and are confined to the core region due to the effect of refractive index guiding. At 1.5 THz, the ERI values for amphetamine, cocaine, ketamine, morphine, NaCN, and KCN are 1.5032, 1.4875, 1.5469, 1.5251, 1.4361, and 1.3971, respectively, which demonstrate the THz wave can confine to the core well.

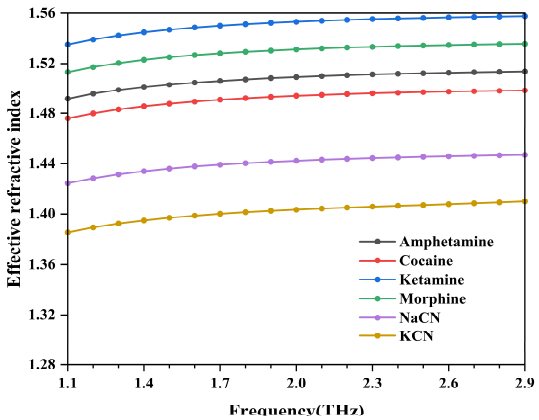

Fig. 6 The ERI versus frequency graph for six chemicals

Fig. 7 shows the relationship between RS and operating frequency for the six analytes. It can be seen that the RSs of the illegal drugs hardly change with increasing operating frequency and remains RS＞99% across the entire range, especially in 2.2-2.9THz. However, the RSs of the cyanides decrease as the frequency increases. This can be explained that the interaction between the cyanides and the THz waves gradually weakens with increasing frequency, since more THz waves distribute in the background due to the smaller refractive index, which lead to decrease of the RS. The RS values for amphetamine, cocaine, ketamine, morphine, NaCN, and KCN are 99.482%, 99.301%, 99.854%, 99.689%, 98.404%, and 97.185% at 1.5 THz, respectively. Compared to Refs [19,21,22], the PCF model designed in this study has a higher RS, making it highly suitable for detecting substances with higher refractive index.

ISSN: 2414-1895 DOI: 10.6919/ICJE.202601_12(1).0003

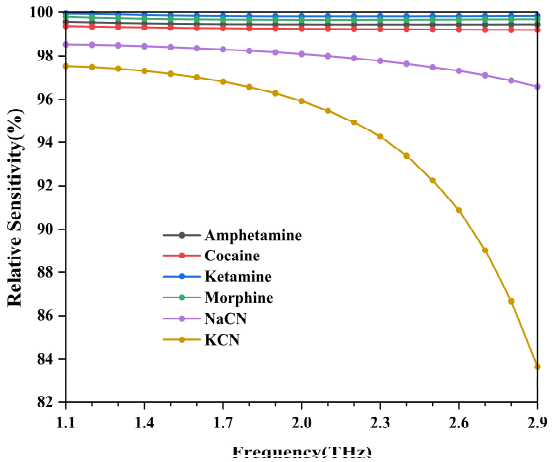

Fig. 7 The RS versus frequency for different chemicals

Fig. 8 depicts the variation of the EML of the analytes with respect to the operating frequency. It can be seen that the EML of the illegal drugs decreases with increasing frequency. This is because high-frequency THz waves tend to propagate more in regions of higher refractive index, allowing the THz wave to interact better with the drug analyte, thereby reducing the EML. The EML of NaCN and KCN shows a tendency to decrease and then increase with increasing frequency. This is due to the fact that KCN has higher material absorption at higher frequencies, agreement with Fig. 7 at higher frequency region, the RSs for cyanide reduce. At 1.5 THz, the EML of amphetamine, cocaine, ketamine, morphine, NaCN, and KCN are 0.003031 cm^{-1}, 0.003362 cm^{-1}, 0.002322 cm^{-1}, 0.002642 cm^{-1}, 0.004934 cm^{-1}, and 0.006985 cm^{-1}, respectively, which are so lower that demonstrates that this PCF can be used to detect these chemicals.

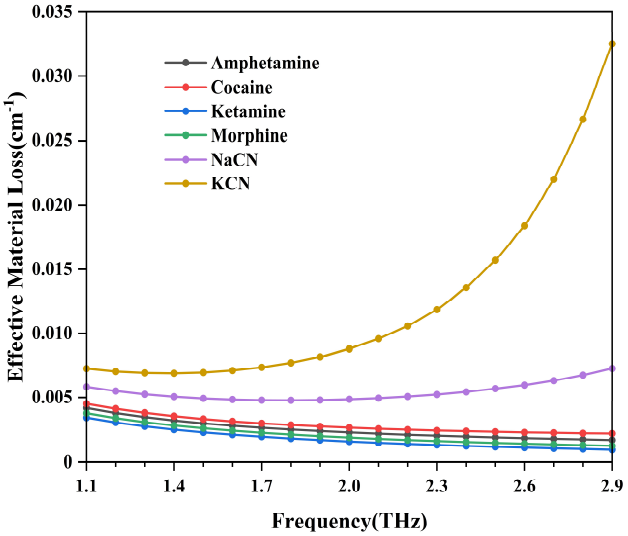

Fig. 8 The variation of EML with frequency

The plot of CL versus frequency is shown in Fig. 9. It can be found that the confinement loss fluctuates randomly as the operating frequency increases. At 1.5 THz, the CL values of amphetamine, cocaine, ketamine, morphine, NaCN, and KCN are 7.15×10^{-15}dB/cm, 8.69×10^{-15}dB/cm, 9.25×10^{-16}dB/cm, 9.12×10^{-16}dB/cm, 4.70×10^{-15}dB/cm, and 31.71×10^{-15}dB/cm, respectively, which indicates the CL of this PCF is almost negligible and this structure of PCF can be used to detect the six chemicals.

ISSN: 2414-1895 DOI: 10.6919/ICJE.202601_12(1).0003

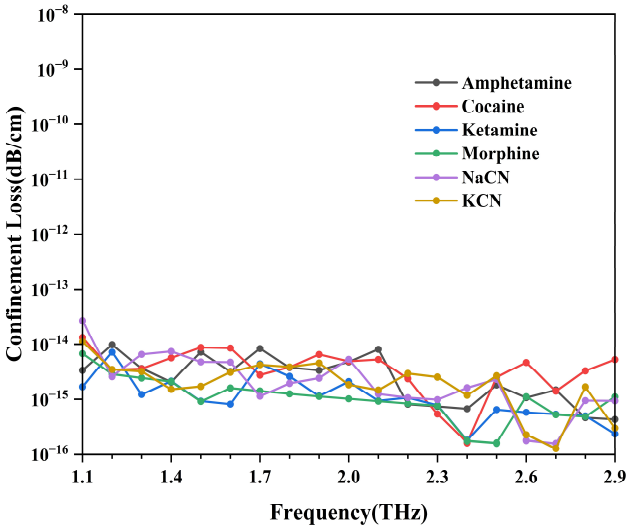

Fig. 9 The relation of CL versus frequency

Fig. 10 depicts the variation of the CPF of the analytes with respect to the operating frequency. The trend shown in this figure is very similar to that in Fig. 7, indicating that the RS is mainly determined by CPF. The CPFs for the illegal drugs increase with increasing frequency while the CPFs for cyanide first increase and then decrease as the frequency increase. The most significant change is observed for KCN at higher frequencies, where the CPF respectively increase slight and drastically decrease in lower and higher frequency region. Because of the large difference in refractive index and material absorption between the illegal drugs and cyanide, which are corresponding with Fig.8, and further can demonstrate the reason of reduction for the RS in Fig. 7. The CPF of amphetamine, cocaine, ketamine, morphine, NaCN, and KCN are 98.273%, 98.072%, 98.698%, 98.507%, 97.100%, and 95.825% at 1.5 THz, respectively, which exceed the results in Refs [19,21,22]

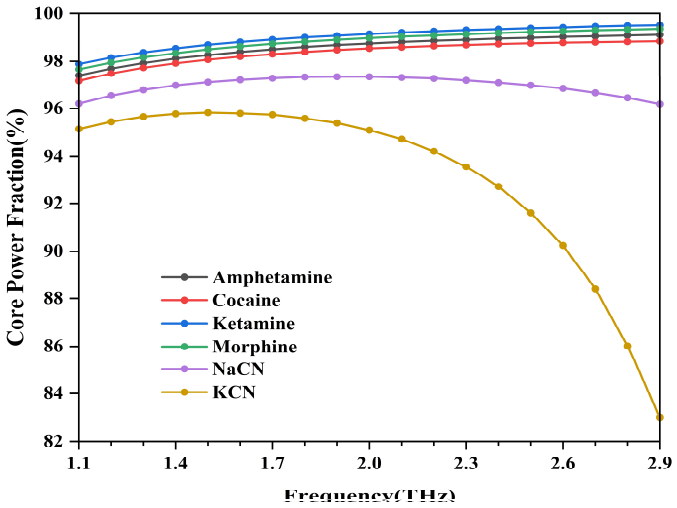

Fig. 10 The CPF versus frequency for different chemicals

The variation of EA versus frequency for the PCF designed is shown in Fig. 11. The EA for the illegal drugs is smaller and decreases with increasing frequency, in which it respectively drops faster and slower in the lower and higher frequency range which indicates the mode field is more concentrated in the core corresponding with Fig. 10. This occurs because THz waves for higher frequency were confined to the core center due to the stronger scattering effect, leading to a decrease in EA, which also explains the reason for the higher RSs in Fig. 7. The EA for cyanide, however, tends to decrease and then increase with rising frequency. This is due to the fact that at higher frequencies, cyanide is

ISSN: 2414-1895 DOI: 10.6919/ICJE.202601_12(1).0003

less effective in limiting THz waves due to its lower refractive index and larger material absorption, leading to an increase in EA as well as a decrease for RS in Fig. 7 and Fig. 10. The EA values for amphetamine, cocaine, ketamine, morphine, NaCN, and KCN are $2.002\times10^{-7}m^2$, $2.041\times10^{-7}m^2$, $1.914\times10^{-7}m^2$, $1.955\times10^{-7}m^2$, $2.214\times10^{-7}m^2$, and $2.418\times10^{-7}m^2$ at 1.5 THz, respectively, which are smaller than that in Ref [21] and approach to that in Ref [22].

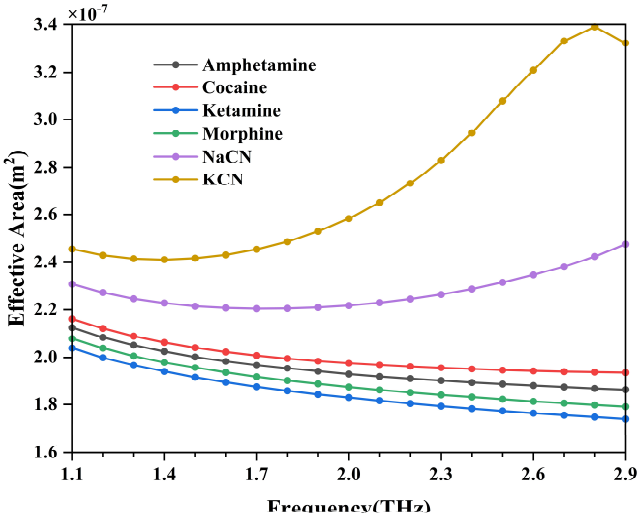

Fig. 11 The EA of PCF versus frequencies

Fig. 12 demonstrates the variation of NA with frequency for the different analytes. In the figure, NA decreases with increasing frequency for all six substances and remains very similar tendency for all of the analytes, in which the variation is larger for the NaCN and KCN. According to equation (9), NA is determined by EA, agree to Fig.11 except for NaCN and KCN at higher frequencies, since the EA mainly depends on the structure and refractive index of material for the fiber. For same frequency of THz wave, the larger the refractive index of the material, the smaller the EA. At 1.5 THz, the NA values for amphetamine, cocaine, ketamine, morphine, NaCN, and KCN are 0.2445, 0.2423, 0.2498, 0.2473, 0.2332, and 0.2237, respectively.

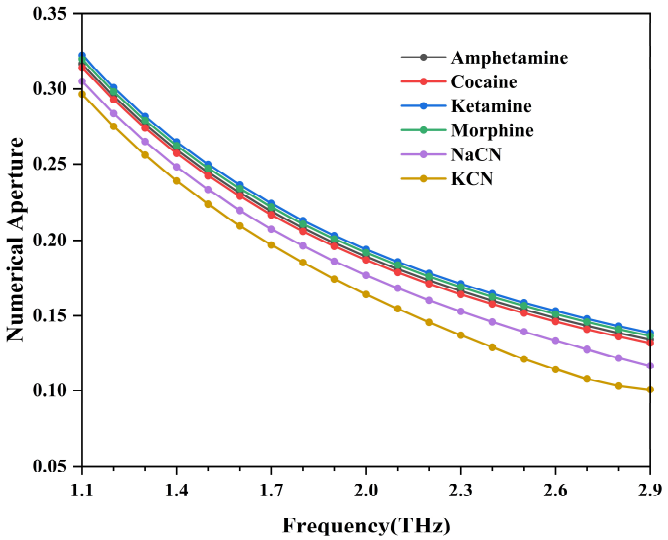

Fig. 12 The NA versus frequency for different chemicals

ISSN: 2414-1895 DOI: 10.6919/ICJE.202601_12(1).0003

To illustrate the capability of the PCF sensing, a comparison is presented in Table 1. From the table, ones can see the proposed PCF exhibits higher RS, lower EML, and higher CPF than other PCF models. Additionally, NA is considered in this paper, whereas it is neglected in refs [19,21,22].

Table 1. Comparison of the proposed PCF's optical characteristics to those of existing PCFs.

Refs	Component name	Background material	Operating frequency	RS (%)	EML (cm^{-1})	CL (dB/cm)	CPF (%)	Aeff (m^2)	NA
[19]2018	HCN	Zeonex	1.8THz	77.5%	0.031	5.15×10^{-9}	-	-	-
	KCN		1.8THz	85.7%	-	-	-	-	-
	NaCN		1.8THz	87.6%	-	-	-	-	-
[21]2020	Amphetamine	Zeonex	1.6THz	92.34%	0.0117	1.402×10^{-15}	-	5.5588×10^{-7}	-
	Cocaine		1.6THz	90.72%	0.0096	2.558×10^{-15}	-	5.6821×10^{-7}	-
	Ketamine		1.6THz	94.91%	0.0149	2.884×10^{-15}	-	5.3143×10^{-7}	-
	Morphine		1.6THz	97.84%	0.0184	0	-	4.7681×10^{-7}	-
[22]2023	Ketamine	Topas	1.0THz	90.20%	-	6.40×10^{-10}	75.05%	1.37×10^{-7}	-
	Amphetamine		1.0THz	89.50%	0.02	6.20×10^{-10}	75.85%	1.40×10^{-7}	-
	Cocaine		1.0THz	85.50%	-	7.10×10^{-10}	74.70%	1.39×10^{-7}	-
This work	Amphetamine	Zeonex	1.5THz	99.482%	0.003031	7.15×10^{-15}	98.273%	1.885×10^{-7}	0.2445
	Cocaine		1.5THz	99.301%	0.003362	8.69×10^{-15}	98.072%	1.944×10^{-7}	0.2423
	Ketamine		1.5THz	99.854%	0.002322	9.25×10^{-16}	98.698%	1.773×10^{-7}	0.2498
	Morphine		1.5THz	99.698%	0.002642	9.12×10^{-16}	98.507%	1.822×10^{-7}	0.2473
	NaCN		1.5THz	98.404%	0.004934	4.70×10^{-15}	97.100%	2.271×10^{-7}	0.2332
	KCN		1.5THz	97.185%	0.006985	1.71×10^{-15}	95.825%	2.430×10^{-7}	0.2237

5. Conclusion

In order to achieve high RS with a simple PCF structure, this paper proposes and analyzes a hexagonal-core PCF for sensing, which features only three cladding air holes and one core structure. This design is easy to fabricate and stable structure. Four illegal drugs-amphetamine, cocaine, ketamine, and morphine-as well as two cyanides, NaCN and KCN, are simulated as analytes to be injected into the fiber core. The sensing and transmission characteristics of this PCF are then calculated and analyzed. Compared to the other results, this PCF exhibits higher RS, lower EML, and higher CPF. The RSs for four illegal drugs increase with rising operating frequency, approach to or even reach to 100% , while for the two cyanides, the RSs respectively increase slowly and decrease rapidly in lower and higher frequency range. To detect the six chemicals, a lower frequency with 1.5 THz is chosen as the operating frequency, and the RSs of 99.482%, 99.301%, 99.854%, 99.698%, 98.404% and 97.185% were achieved for amphetamine, cocaine, ketamine, morphine, NaCN, and KCN, respectively.

Additionally, other properties of the optical fiber, such as EML, CL, CPF, EA, and NA, are also discussed. Compared with recently published PCF models, the proposed PCF for drug and cyanide detection not only demonstrates very high RS but also exhibits very low CL and EML, which contribute to increased sensitivity. This suggests that it may become a new method for illegal drugs and cyanides detection in the future.

Acknowledgments

The authors declare no conflicts of interest.

ISSN: 2414-1895 DOI: 10.6919/ICJE.202601_12(1).0003

References

[1] D. Dragoman, M. Dragoman, Terahertz fields and applications, Progress in quantum electronics 28(2004) 1-66.

[2] P. Mukherjee, B. Gupta, Terahertz (THz) frequency sources and antennas-A brief review, International Journal of Infrared and Millimeter Waves 29(2008) 1091-1102.

[3] M. Zhang, J.T.W. Yeow, Nanotechnology-Based Terahertz Biological Sensing: A review of its current state and things to come, IEEE Nanotechnology Magazine 10(2016) 30-38.

[4] C. Wang, F. Shi, M. Zhao, J. Ao, S. Chen, Convolutional Neural Network-Based Terahertz Spectral Classification of Liquid Contraband for Security Inspection, IEEE Sensors Journal 21(2021) 18955-18963.

[5] J. Yang, L. Qi, B. Li, L. Wu, D. Shi, J.A. Uqaili, X. Tao, A terahertz metamaterial sensor used for distinguishing glucose concentration, Results in Physics 26(2021) 104332.

[6] H Lv, S Li, High sensitivity terahertz biomedical sensing with graphene metamaterial, Optics Communications 566(2024) 130708.

[7] Q. Shangguan, Y. Zhao, Z. Song, J. Wang, H. Yang, J. Chen, C. Liu, S. Cheng, W. Yang, Z. Yi, High sensitivity active adjustable graphene absorber for refractive index sensing applications, Diamond and Related Materials 128(2022) 109273.

[8] R. Wang, J. Han, J. Liu, H, Tian, W, Sun, L. Li, X. Chen, Multi-foci metalens for terahertz polarization detection, Optics Letters 45(2020) 3506-3509.

[9] W. Li, Y. Liu, L. Ling, Z. Sheng, S. Cheng, Z. Yi, P. Wu, Q. Zeng, B. Tang, S. Ahmad, The tunable absorber films of grating structure of AlCuFe quasicrystal with high Q and refractive index sensitivity, Surfaces and interfaces 48(2024) 104248.

[10] P. Knobloch, C. Schildknecht, T. Kleine-Ostmann, M. Koch, S. Hoffmann, M. Hofmann, E. Rehberg, M. Sperling, K. Donhuijsen, G. Hein, Medical THz imaging: an investigation of histo-pathological samples, Physics in Medicine & Biology 47(2002) 3875.

[11] T.A. Birks, J.C. Knight, P.S.J. Russell, Endlessly single-mode photonic crystal fiber, Optics Letters 22(1997) 961-963.

[12] S.A. Razzak, Y. Namihira, M.A. Hossain, A. Khaleque, Designing birefringence ofindex-guiding non-hexagonal photonic crystal fibers, Journal of Optics 40(2011) 56-64.

[13] J.C. Knight, T.A. Birks, P.S.J. Russell, J.P. De Sandro, "Properties of photonic crystal fiber and the effective index model, Journal of the Optical Society of America A 15(1998) 748-752.

[14] X. Yang, Y. Lu, B. Liu, J. Yao, Analysis of graphene-based photonic crystal fiber sensor using birefringence and surface plasmon resonance, Plasmonics 12(2017) 489-496.

[15] T. Wang, Y. Zhou, H. Feng, P. Sun, L. Su, R. Zhao, L. Ran, Y. Gao, Terahertz cancer cell sensor based on plasmonic toroidal metasurface, Optics Communications 575(2025) 131267.

[16] R. Zhou, C. Wang, Y. Huang, K. Huang, Y. Wang, W. Xu, L. Xie, Y. Ying, Label-free terahertz microfluidic biosensor for sensitive DNA detection using graphene-metasurface hybrid structures, Biosensors and Bioelectronics 188(2021) 113336.

[17] H. Yoshida, Y. Ogawa, Y. Kawai, S. Hayashi, A. Hayashi, C. Otani, E. Kato, F. Miyamaru, K. Kawase, Terahertz sensing method for protein detection using a thin metallic mesh, Applied physics letters 91(2007) 253901.

[18] M.S. Islam, J. Sultana, K. Ahmed, M.R. Islam, A. Dinovitser, B.W.H. Ng, D. Abbott, A novel approach for spectroscopic chemical identification using photonic crystal fiber in the terahertz regime, IEEE Sensors Journal 18(2017) 575-582.

[19] M.S. Islam, J. Sultana, A. Dinovitser, K. Ahmed, B.W.H. Ng, D. Abbott, Sensing of toxic chemicals using polarized photonic crystal fiber in the terahertz regime, Optics Communications 426(2018): 341-347.

[20] S.R. Tahhan, H.K. Aljobouri, Sensing of illegal drugs by using photonic crystal fiber in terahertz Regime, Journal of Optical Communications 44(2020) s505-s515.

[21] A.A.M. Bulbul, M.A. Awal, M.E. Rahaman, F. Imam, E. Podder, M.S. Ahmed, M.B. Hossain, H.S. Mondal, F. Iqbal, Highly sensitive photonic crystal fiber for illegal drugs detection in THz regime, 2020

ISSN: 2414-1895 DOI: 10.6919/ICJE.202601_12(1).0003

11th International Conference on computing, communication and networking technologies (ICCCNT). IEEE(2020) 1-6.

[22] M.K. Monir, M.S. Uddin, S. Sen, Design of a novel photonic crystal fiber and numerical analysis of sensitivity for the detection of illegal drugs in terahertz regime, Sensing and Bio-Sensing Research 39(2023) 100551.

[23] E. Lounkine, M.J. Keiser, S. Whitebread, D. Mikhailov, J. Hamon, J.L. Jenkins, P. Lavan, E. Weber, A.K. Doak, S. Cté, Large-scale prediction and testing of drug activity on side-effect targets, Nature 486(2012) 361-367.

[24] S. Erdemir, S. Malkondu, On-site and low-cost detection of cyanide by simple colorimetric and fluorogenic sensors: Smartphone and test strip applications, Talanta 207(2020) 120278.

[25] V.S. Chaudhary, D. Kumar, TOPAS based porous core photonic crystal fiber for terahertz chemical sensor, Optik 223(2020) 165562.

[26] M.S. Islam, J. Sultana, A. Dinovitser, B.W.H. Ng, D. Abbott, A novel Zeonex based oligoporous-core photonic crystal fiber for polarization preserving terahertz applications, Optics Communications 413(2018) 242-248.

[27] A.A.M. Bulbul, F. Imam, M.A. Awal, M.A.P. Mahmud, A novel ultra-low loss rectangle-based porous-core PCF for efficient THz waveguidance: design and numerical analysis, Sensors 20 (2020) 6500.

[28] M. Yamazaki, Industrialization and application development of cyclo-olefin polymer, Journal of Molecular Catalysis A: Chemical 213(2004) 81-87.

[29] I.K. Yakasai, A. Rahman, P.E. Abas, F. Begum, Theoretical Assessment of a Porous Core Photonic Crystal Fiber for Terahertz Wave Propagation, Journal of Optical Communications 43(2022) 199-209.

[30] J.C. Knight, T.A. Birks, D.M. Atkin, P.S.J. Russell, Pure silica single-mode fibre with hexagonal photonic crystal cladding, Optical fiber communication conference. Optica Publishing Group (1996) PD3.

[31] C.M.B. Cordeiro, E.M. Dos Santos, C.H. Brito Cruz, C.J.S. de Matos, D.S. Ferreira, Lateral access to the holes of photonic crystal fibers-selective filling and sensing applications, Optics Express 14(2006) 8403-8412.

[32] S. Atakaramians, S. Afshar V, H. Ebendorff-Heidepriem, M. Nagel, B.M. Fischer, D. Abbott, T.M. Monro, THz porous fibers: design, fabrication and experimental characterization, Optics Express 17(2009) 14053-14062.

[33] I. Ishida, T. Akamatsu, Z. Wang, Y. Sasaki, K. Takenaga, S. Matsuo, Possibility of stack and draw process as fabrication technology for multi-core fiber, 2013 optical fiber communication conference and exposition and the national fiber optic engineers conference (OFC/NFOEC) IEEE(2013) 1-3.

[34] P. Zhang, J. Zhang, P. Yang, S. Dai, X. Wang, W. Zhang, Fabrication of chalcogenide glass photonic crystal fibers with mechanical drilling, Optical Fiber Technology 26(2015) 176-179.

[35] H. El Hamzaoui, Y. Ouerdane, L. Bigot, G. Bouwmans, B. Capoen, A. Boukenter, S. Girard, M. Bouazaoui, Sol-gel derived ionic copper-doped microstructured optical fiber: a potential selective ultraviolet radiation dosimeter, Optics Express 20(2012) 29751-29760.

[36] A. Ghazanfari, W. Li, M.C. Leu, G.E. Hilmas, A novel freeform extrusion fabrication process for producing solid ceramic components with uniform layered radiation drying, Additive Manufacturing 15(2017) 102-112.

[37] H. Ebendorff-Heidepriem, J. Schuppich, A. Dowler, L. Lima-Marques, T.M. Monro, 3D-printed extrusion dies: a versatile approach to optical material processing, Optical Materials Express 4(2014) 1494-1504.

[38] M.R. Sardar, M. Faisal, Methane gas sensor based on microstructured highly sensitive hybrid porous core photonic crystal fiber, Journal of Sensor technology 9(2019): 12-26.

[39] S. Asaduzzaman, K. Ahmed, Proposal of a gas sensor with high sensitivity, birefringence and nonlinearity for air pollution monitoring, Sensing and Bio-Sensing Research 10(2016) 20-26.

[40] M.A. Habib, E. Reyes-Vera, J. Villegas-Aristizabal, M.S. Anower, Numerical modeling of a rectangular hollow-core waveguide for the detection of fuel adulteration in terahertz region, Fibers 8(2020) 63.

[41] A.A.M. Bulbul, R.H. Jibon, S. Biswas, S.T. Pasha, M.A. Sayeed, Photonic crystal fiber-based blood components detection in THz regime: Design and simulation, Sensors International 2(2021) 100081.

ISSN: 2414-1895 DOI: 10.6919/ICJE.202601_12(1).0003

[42] A.M. Maidi, P.E. Abas, P.I. Petra, S. Kaijage, N. Zou, F. Begum, Theoretical considerations of photonic crystal fiber with all uniform-sized air holes for liquid sensing, Photonics 8(2021) 249..

[43] 43. J. Sultana, M.S. Islam, J. Atai, M.R. Islam, D. Abbott, Near-zero dispersion flattened, low-loss porous-core waveguide design for terahertz signal transmission, Optical Engineering 56(2017) 076114-076114.

[44] J. Sultana, M.S. Islam, M.R. Islam, D. Abbott, High numerical aperture, highly birefringent novel photonic crystal fibre for medical imaging applications, Electronics Letters 54(2018) 61-62.